JHEP

Published for SISSA by Springer

Received: November 18, 2018
Accepted: December 30, 2018
Published: January 4, 2019

Non-equilibrium critical phenomena from probe brane holography in Schrödinger spacetime

Ali Vahedi and Mobin Shakeri

Departemet of Physics, Kharazmi University,
Mofatteh Ave, Tehran, Iran
Applied Science Research Center (ASRC),
Kharazmi University, Karaj, Iran

E-mail: vahedi@khu.ac.ir, Mobin.shakeri@live.com

Abstract: We study the non-equilibrium steady-state phase transition from probe brane holography in $z = 2$ Schrödinger spacetime. Concerning differential conductivity, a phase transition could occur in the conductor state. Considering constant current operator as the external field and the conductivity as an order parameter, we derive scaling behavior of order parameter near the critical point. We explore the critical exponents of the non-equilibrium phase transition in two different Schrödinger spacetimes, which originated 1) from supergravity, and 2) from AdS blackhole in the light-cone coordinates. Interestingly, we will see that even at the zero charge density, in our first geometry, the dynamical critical exponent of $z = 2$ has a major effect on the critical exponents.

Keywords: AdS-CFT Correspondence, Gauge-gravity correspondence, Holography and condensed matter physics (AdS/CMT), Holography and quark-gluon plasmas

ArXiv ePrint: 1811.05823

https://doi.org/10.1007/JHEP01(2019)047

JHEP01(2019)047

Contents

1 Introduction 1

2 Non-linear DC conductivity from probe branes 2

3 Probe branes in Schrödinger spacetime from NMT 4
- 3.1 Realization of two states: BH and MEH 6
- 3.2 Negative to positive resistivity: the phase transition 7
- 3.3 Critical exponents 10

4 Probe branes in Schrödinger spacetime from ALCF: strange metal 12
- 4.1 Phase transition and critical exponents 14
- 4.2 Electric field along the light-cone direction 15

5 Notes on numerical calculation 16

6 Conclusion 17

JHEP01(2019)047

1 Introduction

Believing the holographic principle, holographic probe branes give us an analytic description of the non-linear electric conductivity of strongly coupled QFTs [1, 2]. The N_f $D7$-branes as a probe, in the background of N_c $D3$-branes introduce the fermions(and anti-fermions) in the dual theory with fundamental(and anti-fundamental) representation of supersymmetric $\mathcal{N} = 2$, which localized on a defect sector within the background plasma, $\mathcal{N} = 4$ supersymmetric Yang-Mills theory. The null Melvin twist(NMT) transformation of this configuration, will produce the extension of the holographic probe branes on the Schrödinger background [4]. It was convincing that Schrödinger geometry, in general, is dual to the theory of cold fermions at unitarity [5, 6].[1] As well as the NMT transformation, it was shown that the isometry of AdS geometry in the light-like coordinate will also reduce to the Schödinger group [7, 8]. Holographic probe branes in the AdS metric at the light-cone frame(ALCF), for the non-zero charge density, might establish a framework to study Strange metal [9, 10]. Beside the two form B-field, at zero temperature, both Shrödinger background from ALCF and NMT transformation have the metric with the $z = 2$ dynamical critical exponent. The B-field will break the SUSY in the solution derived from NMT procedure, therefore, in general, they have different dual theories. Note that

[1] As mentioned in [4], Type IIB string theory in Schrödinger background is not exactly a dual to the theory of fermions at unitarity. Although, the correlation functions, especially the three-point function, from holographic approach are in agreement with the three-point function of fermions at unitarity, see for example [25, 26].

the QFT with Schrödinger symmetry which created by the above transformations lives in one dimension lower than its original QFT with conformal symmetry.

By turning an electric field on the probe D-brane, the world-volume horizon will emerge and we can assign a temperature to this horizon. This temperature, is generally distinct from the background temperature. This means that (anti-)particles in the (anti-)fundamental representation dual theory live in a state with a different temperature from the background plasma(adjoint representation). Therefore, the system is standing at a non-equilibrium steady state, see [21–23] for detailed discussion. In other words, the electric field pumps energy into the fermions(flavors) sector and then it dissipates into the background plasma, see also [24].Hence, the system is in out of equilibrium. Non-linear differential conductivity of systems in a non-equilibrium steady state is studied from holographic probe branes in the AdS background at [14–16]. It was shown that the sign of the differential conductivity could be changed from negative to positive. The continuous (second order), first-order phase transitions and crossover from negative differential conductivity(NDC) to positive differential conductivity (PDC) are studied in [14–17]. Also in [15, 17, 18], the order parameters of non-equilibrium steady state at the critical point are proposed and their scalings are investigated.

According to the bulk theory for other geometries, the mechanism that makes the system out of equilibrium is similar to the AdS background. In this work, we are going to study the non-equilibrium steady state in Schrödinger background with $z = 2$ dynamical critical exponent. We investigate and compare the NDC to PDC phase transitions in the both Schrödinger spacetime, ALCF and NMT.

2 Non-linear DC conductivity from probe branes

Consider a strongly correlated QFT with emerging Schrödinger symmetry at its critical point and conserved U(1) current J^a. The Schrödinger symmetry admits Lifshitz scaling

$$t \to \lambda^z t\,, \qquad \vec{x} \to \lambda \vec{x}, \tag{2.1}$$

where z is known as dynamical critical exponent. For $z = 2$, the holographic dual to this theory could be N_f $D7$-branes probing the background with null Melvin twist(NMT) of $AdS_5 \times S^5$ [4, 13] or $AdS_5 \times S^5$ in light-cone frame(ALCF) [9] with non-zero A_a gauge field on the $D7$-branes. As mentioned, the N_f $D7$-branes will be treated as probes in the background of N_c D3-branes. Thus, the dynamics of the system is given by the Dirac-Born-Infeld(DBI) action for $D7$-branes:[2]

$$S_{D7} = -\mathcal{N}\int dr\; e^{-\Phi}\sqrt{-\det\left(P\left[g+B\right]_{ab} + (2\pi\alpha')\,F_{ab}\right)}\,, \tag{2.2}$$

where $\mathcal{N} = 2\pi^2 N_f T_{D7}$, and $P[g+B]_{ab}$ stands for pullback or induced metric and induced two-form B-field on the D7 branes. The F_{ab} is a gauge field stress tensor on the probe branes. To extract the equations of motion from eq. (2.2), we assume the embeddings as table 1 for the probe $D7$-branes.

[2]There is also the Wess-Zumino action term, which for our embedding is zero. We also normalized the action with $D3$-branes world-volume.

JHEP01(2019)047

	x^+	x^-	x ,y	r	σ_α or S^3	θ	χ
D3	×	×	×				
D7	×	×	×	×	×		

Table 1. $D3-D7$ embedding.

As it is clear, There is $O(2)$ symmetry along (θ,χ). Without loss of generality, we make the assumption that $\theta=\theta(r)$ and $\chi=0$. We assume the following gauge fields on the probe branes,[3]

$$2\pi\alpha' A_x(x^+,x^-,r)=E_b x^+ - b^2\,E_b\,x^- + a_x(r) \tag{2.3}$$

which E_b is a constant non-relativistic electric field. We consider zero charge density,[4] so with this ansatz, we have two equations of motion for A_a and $\theta(r)$ to solve:

$$\frac{d}{dr}\frac{\partial\mathcal{L}}{\partial a'_x}=0 \qquad or \qquad \frac{\partial\mathcal{L}}{\partial a'_x}=D\,, \tag{2.4}$$

$$\frac{\partial\mathcal{L}}{\partial\theta}-\frac{d}{dr}\frac{\partial\mathcal{L}}{\partial\theta'}=0\,, \tag{2.5}$$

where the prime stands for the derivative relative to r. At the near boundary $r=0$ the solutions of eq. (2.4) would be

$$a_x(r)\approx c+\frac{\langle J^x\rangle}{(2\pi\alpha')^2\mathcal{N}}\,r^2+\dots\,, \tag{2.6a}$$

where from guage-gravity dictionary [2], $\langle J^x\rangle = D$. The near boundary solution of eq. (2.5) is

$$\theta(r)\approx 2\pi\alpha' m_q\,r+\frac{\langle\bar\psi\psi\rangle}{\mathcal{N}}\,r^3+\dots \tag{2.6b}$$

or

$$2\pi\alpha' m_q=\lim_{r\to0}\frac{\theta(r)}{r} \tag{2.6c}$$

where m_q is a flavor's(quark's) mass. From eq. (2.4), we could find the on-shell action and also Legendre transform of the action, $\tilde{\mathcal{L}}=\mathcal{L}-A'_x\frac{\partial\mathcal{L}}{\partial A'_x}$.

For zero gauge fields on the probe branes, there are two embeddings. Minkowski embedding (ME) and the black hole embedding(BE). In the bulk theory, for the adequately small ratio of flavor's mass and background Hawking temperature i.e., $\frac{m_q}{T}$, the BE is thermodynamically preferred and for the sufficiently large values of $\frac{m_q}{T}$ the ME is favorable [19, 20].

For the non-zero electric field E_b, larger than the critical value[5] E_b^c, we able to calculate the electric conductivity $\langle J^x\rangle=\sigma\,E_b$, from the reality condition of the DBI action. In other

[3]This is the same gauge field which is introduced to AdS background,i.e.,$E\,t+a_x(r)$, in the light-like coordinates, which $E_b=\frac{E}{2\,b}$.

[4]For non-zero finite charge density see [4, 9, 10].

[5]Which is order of effective string tension on the probe branes.

JHEP01(2019)047

words, for $E_b > E_b^c$ there would be a non-zero current $\langle J^x \rangle$ hence, we have a conductor state and for $E_b < E_b^c$ we live in an insulator state, since $\langle J^x \rangle = 0$. The phase transitions may happen from the insulator state to the conductor state. The presence of the electric field will introduce the world-volume horizon on the probe branes, which in general, differs from the background event horizon. This makes another class of embedding in addition to the Minkowski and the black hole embeddings. Following [16], we call it Minkowski with the horizon embedding(MHE). The Minkowski embedding(ME), in the bulk side, corresponds to the states with $\langle J^x \rangle = 0$, which means that the electric field does not have enough strength to rip off the strings and the bound between the charge carrier pairs would be stable. Differently, the states with $\langle J^x \rangle \neq 0$ is demonstrated by the BE or the MHE. According to our numerical calculation, we will see that for a fixed electric field there would be two non-zero currents. Therefore, in the conductor state the phase transitions may also happen. In the following sections, we investigate the other phase transitions in conductor states through the study of non-linear DC conductivity for a QFT with $z = 2$ Schrödinger symmetry.

3 Probe branes in Schrödinger spacetime from NMT

We consider N_f D7 branes in the below background

$$\begin{aligned} ds^2 = \frac{1}{r^2 K}\left[\left(\frac{f}{r^2} - \frac{1-f}{4b^2}\right)dx^{+2} + \big(1+f\big)dx^+dx^- + \big(1-f\big)b^2dx^{-2}\right] \\ + \frac{1}{r^2}\left[d\vec{x} + \frac{dr^2}{f}\right] + \frac{1}{K}\left(d\chi + \mathcal{A}\right)^2 + ds^2_{\mathbb{CP}^2}\,, \end{aligned} \tag{3.1}$$

where

$$f = 1 - \frac{r^4}{r_H^4}\,, \qquad K = 1 + \frac{b^2 r^2}{r_H^4}\,. \tag{3.2}$$

In addition to this metric, there is a dilatonic scalar field,

$$\Phi = -\frac{1}{2} Log\, K\,, \tag{3.3}$$

and there is also two-form B-field,

$$B = -\frac{1}{2r^2 K}\left(d\chi + \mathcal{A}\right) \wedge \left(\left(1+f\right)\, dx^+ + \left(1-f\right) 2b^2 dx^-\right)\,. \tag{3.4}$$

In this spacetime event horizon located at r_H and the boundary at $r = 0$. This geometry is holographic dual to the thermal quantum state which lives in the temperature equal to the background Hawking temperature. The momentum along the x^- in the dual boundary theory, which is discrete, is number operator generator of Schrödinger algebra. In the gravity side this means we might have preformed DLCQ along the x^-. So the boundary dual theory also has a chemical potential μ,[6] see [4], with

$$T = \frac{1}{\pi\, b\, r_H}\,, \qquad \mu = \frac{-1}{2\, b^2}\,. \tag{3.5}$$

[6]This quantity should not be confused with chemical potential due to U(1) baryon number of flavor fermions.

JHEP01(2019)047

At the zero temperature (or $r_H \to \infty$) the metric of eq. (3.1) changes to

$$ds^2 = \frac{1}{r^2}\left(-\frac{1}{r^2}dx^{+2} + 2dx^+dx^- + d\vec{x}^2 + dr^2\right) + (d\chi + \mathcal{A})^2 + ds^2_{\mathbb{CP}^2} \tag{3.6}$$

which respects the scale invariant as follows

$$x^+ \to \lambda^2 x^+ \quad , \quad \vec{x} \to \lambda\vec{x} \quad , \quad x^- \to \lambda^0 x^- \, , \quad r \to \lambda r \, . \tag{3.7}$$

Comparing the above metric with scaling of eq. (2.1), in here, we deal with the dynamical critical exponent $z = 2$.

The Legendre transformation of DBI action eq. (2.2) would be[7]

$$S_{D7} = \int \tilde{\mathcal{L}}\, dr = -\int_0^{r_H} dr g_{rr}^{1/2}\sqrt{U(r)\,V(r)}. \tag{3.8}$$

where we have defined:

$$g_{rr} = \frac{1}{r^2 f(r)} + \theta'^2 \tag{3.9}$$

$$U(r) = \frac{-4b^2r^2E_b^2\left(r^2 - b^2 f(r)\sin^2\theta\right) + f(r)}{r^2\, f(r)}$$

$$V(r) = \frac{\mathcal{N}^2 f(r)\cos^6\theta}{64r^6} - \langle J^x\rangle^2 \, . \tag{3.10}$$

U and V, in eq. (3.8), can be positive or negative. The reality condition of the action force us to have a special point, r_*, which at this point, U and V change their sign, simultaneously. This means that

$$V(r_*) = 0 \to \langle J^x\rangle^2 = \frac{\mathcal{N}^2 f(r_*)\cos^6\theta(r_*)}{64r_*^6}, \tag{3.11}$$

$$U(r_*) = 0 \to E_b^2 = \frac{f(r_*)}{4\, b^2\, r_*^2(r_*^2 - b^2 f(r_*)\sin^2\theta(r_*))} \, . \tag{3.12}$$

Following open string metric approach to DBI action we could say that the r_* is a location of world-volume (or apparent) horizon [11, 19–21, 24] and we could assign this point an effective temperature, see for detail [22, 23]. Also, from eq. (3.11) and eq. (3.12), one might say that we able to assign a geometric meaning to the electric field, see also [11]. It is clear from eq. (3.12), at the zero electric field $r_* = r_H$ therefore, as already discussed, we summarize the embeddings as follows

$$\text{Embedding classes} = \begin{cases} r_H > r_* > r_\alpha & \text{for ME} \\ r_H > r_\alpha > r_* & \text{for MEH} \\ r_H \geq r_* & \text{for BE} \end{cases} \tag{3.13}$$

where r_α is a shrinking point of the compact coordinates of the probe branes. In the ME the flavor pairs bound is stable, which means current $\langle J^x\rangle$ is zero hence the system lives

[7] See [13]. The Legendre transformation make current J as a controlling parameter [14].

JHEP01(2019)047

as an insulator. The non-zero current exist for both MEH and BE. Consequently, they are signs of conductor state of a system. In the following, we show that the phase transitions could occur in the conductor state.

Before going further, let us focus on eq. (3.11) and eq. (3.12). We could simply drive a formula for the conductivity[8]

$$\langle J^x \rangle = \sigma\, E_b \to \sigma = \frac{\mathcal{N}\, b \cos^3\theta(r_*)}{4r_*^2}\sqrt{r_*^2 - b^2\sin^2\theta(r_*) f(r_*)}\ . \tag{3.14}$$

This is non-linear DC conductivity, since r_* and $\theta(r_*)$ are functions of E_b(and $\langle J^x \rangle$), which can be inferred from eq. (3.11) and eq. (3.12). This is a dimensionless quantity as it was expected to be, in non-relativistic $z = 2$ theory [4]. As mentioned before, the conducting states exist for BE and MEH. To illustrate this statement we focus on $E - J$(V-I or Ohm's law) plot by solving the Euler-Lagrangian equation numerically for $\theta(r)$, in the next section.

3.1 Realization of two states: BH and MEH

In the AdS background, it was shown that the Euler-Lagrange equation could be solved by the initial conditions at the point r_* [14–17]. To solve the second order equation eq. (3.15), we need two initial or boundary conditions. Following [14, 15], we choose our initial conditions at $\theta(r_*)$ and $\frac{d\theta}{dr}(r_*) = \theta'(r_*)$. For the $\theta(r_*)$, we pick one value from $0 < \theta(r_*) < \pi/2$. To choose the right value for $\theta'(r_*)$ we expand $\theta(r)$ near the r_* as

$$\theta(r) = \theta(r_*) + (r - r_*)\theta'(r_*) + \dots \quad . \tag{3.15}$$

Inserting eq. (3.15) into the Euler-Lagrange Equation, with the help of eq. (3.11) and eq. (3.12), we will find $\theta'(r_*)$.[9] Now we can solve the Euler-Lagrange Equation, and from the solution we are able to read the mass of flavors from

$$2\pi\alpha' m_q = \lim_{r\to 0}\frac{\theta(r)}{r}\,. \tag{3.16}$$

With a fixed external electric field E_b, we are able to draw the relation of the flavor's mass to the current J. The result is figure 1, for a fixed background temperature, and a fixed chemical potential.[10] From figure 1, we find the same behavior as $m - J$ plot in the AdS background [14–16].

There is a region where for one value of flavor's mass, we have two different values for current J. This is the same statement as saying the both embedding, MEH and BE, could exist for non-zero current. We also, see that for example, at $E = 0.05$, for $m > 1.31401$ the current does not exist, therefore, flavor pairs have a stable bound, and the embedding is ME. In general, there exists a $m_{\max}$, where for $m > m_{\max}$, the system lives in ME. For $m < m_{\max}$, for the small current region, we have both thermal solutions MEH and BE.

[8] In general, because of the square root, there is a $\pm$ for the conductivity, but without lose of generality, we pick the positive sign.

[9] Which due to the long and cumbersome expressions which lead to it, we avoid writing it explicitly.

[10] For the sake of simplicity, from numerical viewpoint and from (3.5), we use b instead of chemical potential.

JHEP01(2019)047

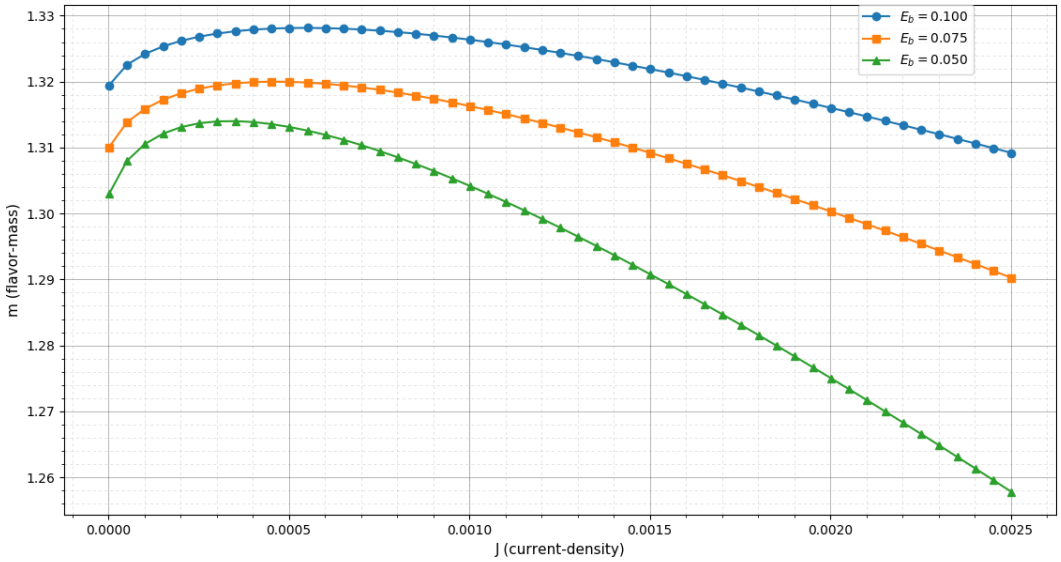

Figure 1. m_q-J curve for different values of E_b at $T = 0.45015$ and $b = 1$. the maximum values are located at $m_{\max} = 1.32813$, 1.32000, and 1.31401; from top to bottom respectively.

As has been already told, this resembles the results in the AdS-Schwarzschild background, except that in the Schrödinger solution, we could change chemical potential μ or b. As it was previously mentioned, the states in the dual QFT are also labeled with a chemical potential in Schrödinger backgrounds, in addition to the temperature. So studying the phase transitions by changing the chemical potential for a fixed temperature will make sense. Hence, both temperature and chemical potential, separately, could control the stable and non-stable states of different embeddings. These different states in the conducting state, with a different current density and an equal flavor's mass, motivate us to study the phase transition.

Note that if we recall the relativistic electric field through $E = 2\,b\,E_b$, for a fixed value of E_b, the lower b results in a smaller E, and the maximum mass would take a smaller value relative to the higher b (see figure 2). This is quite similar to the AdS result. This means that the chemical potential μ or b has a major effect on the distances between D3-and D7 branes, or mass of flavors.

3.2 Negative to positive resistivity: the phase transition

As it was previously pointed, we are dealing with a non-equilibrium steady state, Therefore, in below, we are going to study the non-equilibrium phase transition. By fixing the mass of flavors, we are able to sketch the (E_b -J)'s plot.

For the different values of temperature and a fixed chemical potential μ (or b), we would have figure 3. As it is clear from the figure 3, For the background temperature $T = 0.45015$, the differential conductivity changes continuously by increasing the current density. In the small current region, we have a negative differential conductivity (NDC), and for the higher currents, we have positive differential conductivity(PDC). This is a continuous change or a crossover, from NDC state to PDC state. Moreover, the electric field has a lower bound,

JHEP01(2019)047

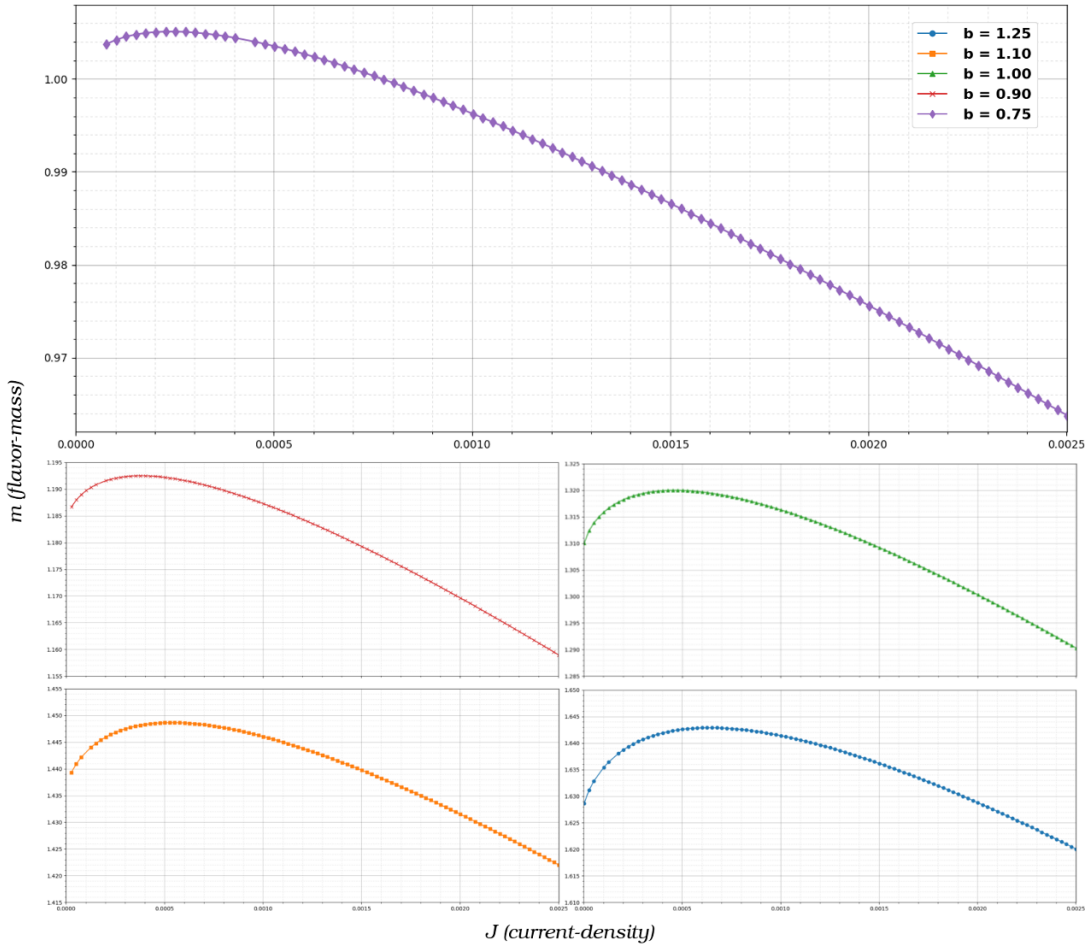

Figure 2. m_q-J curve for different values of b at $T = 0.45015$ and $E_b = 0.15$. the maximum values are located at $m_{\max} = 1.64289, 1.44865, 1.32000, 1.19248, 1.00509$; from high to low b, respectively.

which we call it E_b^c. For example, for $T = 0.45015$ we have $E_b^c = 1.1$. For $E < E_c$ the current is zero which means the Minkowski embedding exists there.

For $T = 0.45240$, in a region with a small current density, there are points with the same value of currents and different electric fields, i.e., points B,C,D. Since the system lives in a non-equilibrium state, following [14, 17], we define energy or non-equilibrium thermodynamic potential, to find out which one is energetically(or thermodynamically) preferable, as:

$$\mathcal{F}(T, b, J; m_q) = \lim_{\epsilon \to 0} \left(\int_{\epsilon}^{r_H} dr\, \mathcal{H} - \mathcal{H}_c(\epsilon) \right) \tag{3.17}$$

where

$$\mathcal{H} = -\mathcal{L}_{\text{eff}} + \partial_\tau A_x \left(\frac{\partial \mathcal{L}_{\text{eff}}}{\partial\, \partial_\tau A_x} \right) = \frac{g_{rr}^{1/2}}{r^2} \left(\frac{V}{U} \right)^{1/2} \tag{3.18}$$

and $\mathcal{H}_c(\epsilon)$ is the counter term for renormalization of the Hamiltonian or effective action.[11]

[11] For holographic renormalization in Schrödinger background see [27, 28]. In here we carefully did the regularization numerically.

JHEP01(2019)047

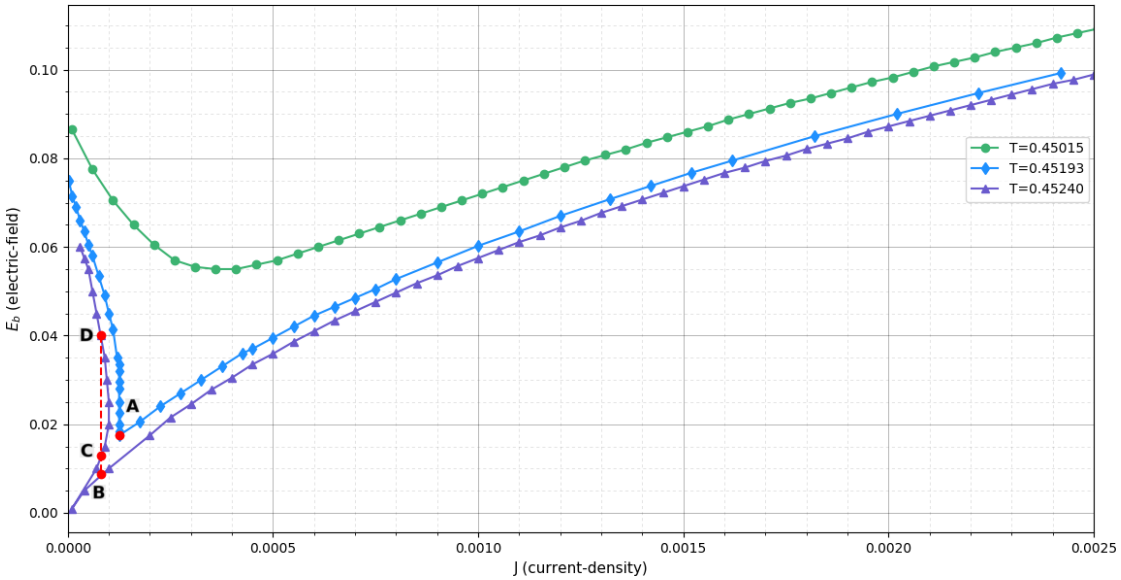

Figure 3. E_b-J curve for different values of T at $m_q = 1.315$ and $b = 1$. the $T_c = 0.45193$ is the critical temperature at this setting.

In contrary to the AdS [14, 15], and similar to the AdS result in the presence of a constant magnetic field [16], the point with largest electric field is favorable. So there would be a jump from the NDC branch (point D) to the PDC branch. We call this discontinuity of conductivity (or the electric field) first order phase transition.

For the temperature $T = 0.45193$ we see that there is a point near A that $\frac{\partial E_b}{\partial J} = \infty$.[12] Consequently, the NDC to PDC transition is a continuous, or a second order phase transition. We call this temperature the critical temperature T_c. At the critical point, the conductivity has a finite quantity, but the differential conductivity is a singular quantity, which means that between the small current region with a negative differential conductivity (NDC), and the larger current region, with a positive differential conductivity (PDC), a continuous phase transition will occur.

In the case of Schrödinger spacetime, we can also change the chemical potential, or b, with a fixed temperature. The same behaviour of phase transition occurs due to the variation of the chemical potential, see figure 4. For $b = 1.003954$ the second order phase transition occurs, where at a point near A, $\frac{\partial E_b}{\partial J} = \infty$. Thus we call the chemical potential of that curve: *critical chemical potential* μ_c (equally b_c). For $b > b_c$, the electric field, hence the conductivity feels discontinuity, so likewise, the first order phase transition would happen.

Concluding from above, we can see that the second order phase transition may occur for different values of b and T. We can express this by saying that the critical temperature is controlled by b and vice versa. Therefore, we may have the critical temperature as a function of b , $T_c(b)$, so a *multicritical point* might exist and the system at that point, might belong to a universality class different from normal universality. Due to the numerical difficulties we postpone the study for multicritical point to the future works. In the

[12] Or $\frac{\partial J}{\partial E_b} = 0$.

JHEP01(2019)047

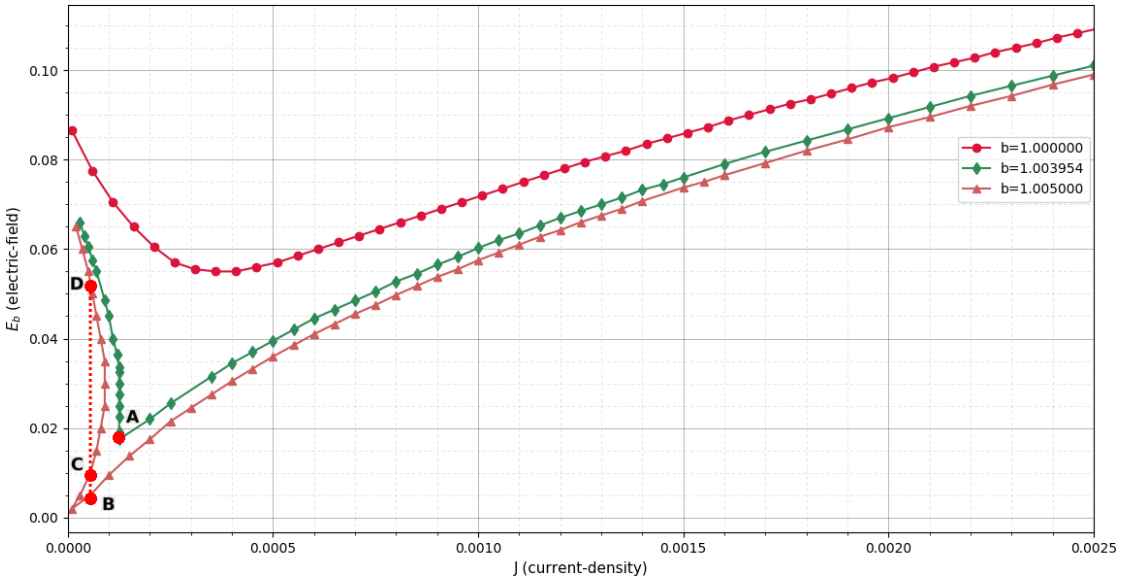

Figure 4. E_b-J curve for different values of b at $m_q = 1.315$ and $T = 0.45015$. the $b_c = 1.003954$ is the critical b at this setting.

meanwhile, we can define

$$\tilde{T} = \frac{T - T_{\text{ref}}}{T_c - T_{\text{ref}}} \qquad \& \qquad \tilde{\mu} = \frac{\mu - \mu_{\text{ref}}}{\mu_c - \mu_{\text{ref}}}. \tag{3.19}$$

Using these, we can represent figure 5, which shows the relation between $\tilde{T}$ and $\tilde{\mu}$. As it was stated above, and from figure 5, by increasing b or chemical potential, the critical temperature decreases. This is quite opposite to the magnetic effect on the critical temperature, see [16].

3.3 Critical exponents

In the meanwhile of studying the phase transition, we can ask about the scaling behaviour of the order parameters near the critical point. Considering $\sigma - \sigma_c$, along the second order phase transition line $T = T_c$, as an order parameter similar to Landau theory [17], we can define

$$\sigma - \sigma_c \propto |J - J_c|^{\frac{1}{\delta_{\text{Sch}}}}, \tag{3.20}$$

where in here, δ_{Sch} is given by the slop of figure 6.

$$\delta_{\text{Sch}} = 1.54 \pm 0.1 \tag{3.21}$$

Interestingly, this is nearly *half* the result in the AdS spacetime [17]. This observation, makes us propose that dynamical exponent z plays a role in here, and we have in general,[13]

$$\sigma - \sigma_c \propto |J - J_c|^{\frac{1}{\delta_z}}, \tag{3.22}$$

[13]We are starting to study a more general scale invariant theory with dynamical critical exponent z [29].

JHEP01(2019)047

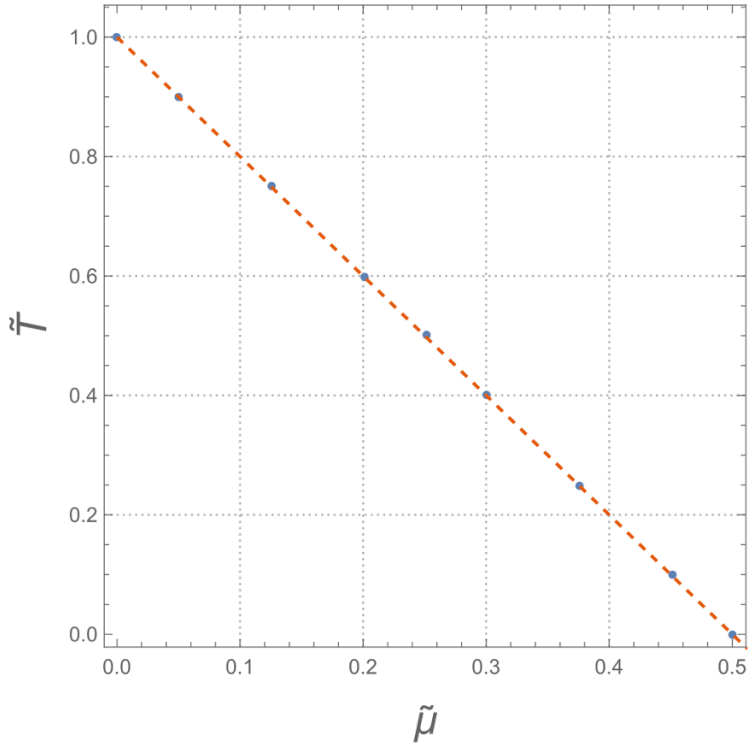

Figure 5. Points of different critical states (second order phase transitions) at different $\tilde{T}$ & $\tilde{\mu}$.

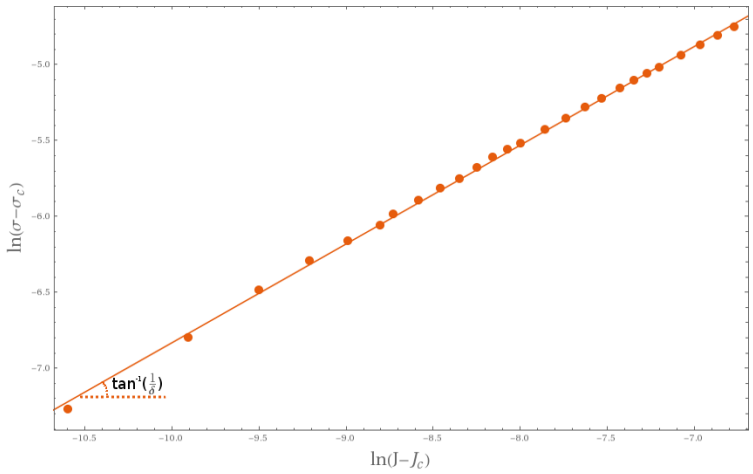

Figure 6. Behaviour of $\ln(\sigma - \sigma_c)$ with the different values of $\ln(J - J_c)$, represnting critical exponent of δ in Schrödinger spacetime. $\delta = 1.54 \pm 0.1$ is computed from the slope of the line presented in the figure.

where we have introduced

$$\delta_z = \frac{\delta_{\text{AdS}}}{z} \,. \tag{3.23}$$

Particularly, this means that at the critical point, we live in a scale-invariant theory with dynamical critical exponent $z = 2$. Within our numerical resolution, the same behavior of eq. (3.20) would be predicted along the $b = b_c$ curve, with the same δ_{Sch}.

JHEP01(2019)047

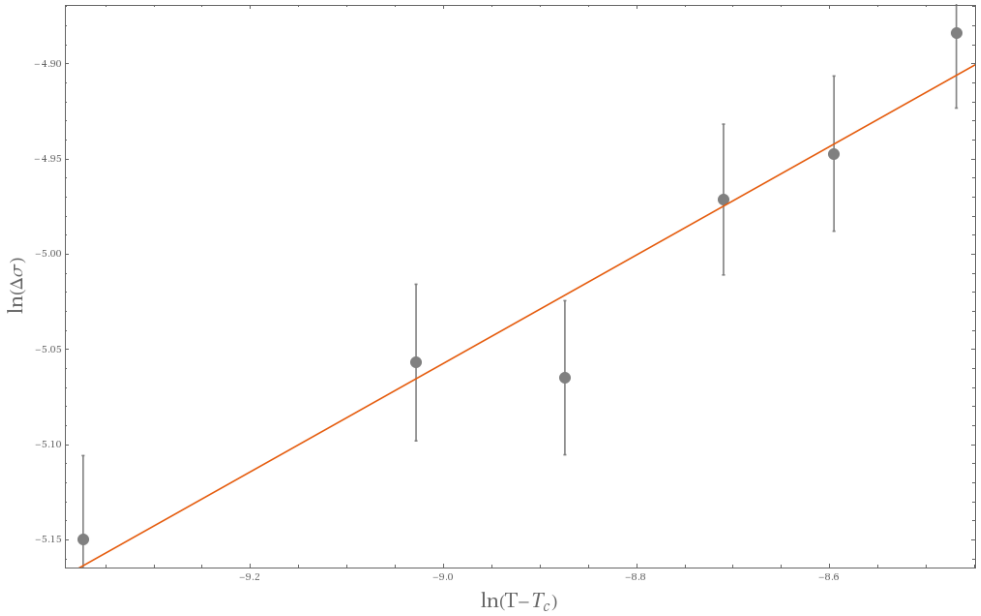

Figure 7. Behaviour of $\ln(\Delta\sigma)$ with the different values of $\ln(T-T_c)$, represnting critical exponent of β in Schrödinger spacetime. $\beta = 0.28 \pm 0.1$ is computed from the slope of the line presented in the figure.

Alongside the first order phase transition lines with $T > T_c$, we can follow [17] to derive the other non-equilibrium critical exponents which has been previously defined as

$$\Delta\sigma \approx |T - T_c|^{\beta} . \tag{3.24}$$

Interestingly, numerical results fluctuate around half the result which is calculated for AdS one, $\beta = 0.28 \pm 0.1$. But yet, there exists some level of doubt in the results, due to the numerical difficulties. This result also supports our point that dynamical exponent of z plays an important role in determining the critical exponents. The same argument is true at a constant temperature, for $\Delta\sigma \approx |\mu - \mu_c|^{\beta}$, from the figure 4.

Results for the critical exponent of γ, which is also defined in [17], is postponed to the future works for a further investigation, due to the difficulties arised from the initial definition of this critical exponent.

4 Probe branes in Schrödinger spacetime from ALCF: strange metal

Let us start with an $AdS_5 \times S^5$, in the unit of AdS radius,

$$ds^2 = \frac{1}{r^2}\left(-f(r)dt^2 + dx^2 + dy^2 + dz^2 + \frac{dr^2}{f(r)}\right) + d\Omega_5^2 \tag{4.1}$$

where $f(r) = 1 - \frac{r^4}{r_H^4}$ and the S^5 metric is

$$d\Omega_5^2 = d\theta^2 + \sin^2\theta d\psi^2 + \cos^2\theta d\Omega_3^2. \tag{4.2}$$

JHEP01(2019)047

The AdS metrics in the light-cone coordinate

$$x^+ = b(t+y) \qquad and \qquad x^- = \frac{1}{2b}(t-y), \tag{4.3}$$

changes to the metrics of ALCF [7, 8], which would be

$$ds^2 = \frac{1}{r^2}\left(\frac{1-f}{4b^2}dx^{+2} - (1+f)dx^+dx^- + (1-f)b^2dx^{-2} + dx^2 + dz^2 + \frac{1}{f}dr^2\right) + d\Omega_5^2\,. \tag{4.4}$$

The event horizon, located at r_H, is related to the temperature through $r_H = \frac{1}{\pi\, b\, T}$. This metric interpolates between AdS $z = 1$, and $z = 2$ Schrödinger symmetry [7–9].

We turn on electric field along x^+ as

$$A_+ = E_b x, \quad A_- = 2b^2 E_b x, \quad A_x = 2E_b b^2 x^- + h_x(r). \tag{4.5}$$

or

$$A_x = -E_b x^+ + h_x(r). \tag{4.6}$$

The Legendre transform of the DBI action is

$$S_{D7} = -\int_0^{r_H} dr\, g_{rr}^{1/2}\sqrt{U(r)\,V(r)}, \tag{4.7}$$

where in here, we have the same $g_{rr}(r)$ as eq. (3.9), and

$$\begin{aligned} U(r) &= \frac{g_{xx}\left(g_{+-}^2 - g_{++}g_{--}\right) - E_b^2 g_{--}}{g_{+-}^2 - g_{++}g_{--}} \\ V(r) &= \frac{\mathcal{N}^2 f(r)\cos^6\theta}{r^6} - \langle J^x\rangle^2\,. \end{aligned} \tag{4.8}$$

The world-volume horizon located at r_*, where both U and V met zero,

$$V(r_*) = 0 \to \langle J^x\rangle^2 = \frac{\mathcal{N}^2 f(r_*)\cos^6\theta(r_*)}{r_*^6}, \tag{4.9a}$$

$$U(r_*) = 0 \to E_b^2 = \frac{f(r_*)r_H^4}{b^2\, r_*^8}\,. \tag{4.9b}$$

Therefore, the electric DC conductivity is

$$\sigma = \frac{\mathcal{N}\, b\, r_*\cos^3\theta(r_*)}{r_H^2}. \tag{4.10}$$

Due to the electric field dependency of r_* and $\theta(r_*)$, this is a non-linear conductivity. The eq. (3.14) has an extra term, $b^2 f(r_*)\sin^2\theta(r_*)$, comparing to eq. (4.10).

For a non-zero charge density we have to add $h_+(r)$ and $h_-(r)$ to A_+ and A_-, respectively. In this case we would have

$$\sigma = \sqrt{\sigma_1 + \sigma_2}, \tag{4.11}$$

JHEP01(2019)047

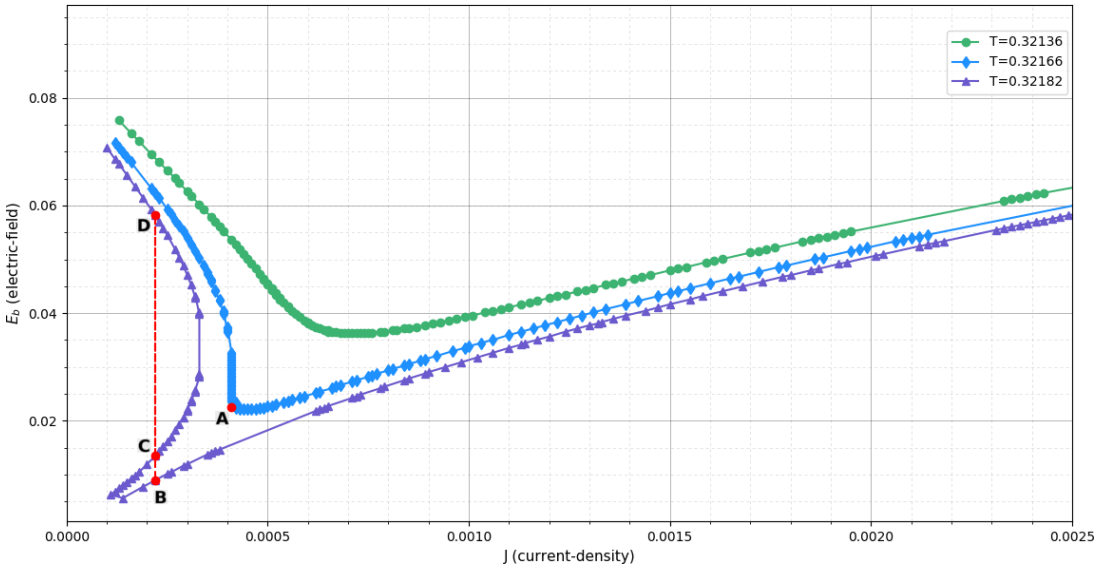

Figure 8. E_b-J curve for different values of T at $m_q = 0.936$ and $b = 1$ of the Strange metal. the $T_c = 0.32166$ is the critical temperature at this setting.

where σ_1 is given by the eq. (4.10), and $\sigma_2 \approx \frac{\langle J^+ \rangle}{g_{xx}(r_*)}$, where $\langle J^+ \rangle$ is a our charge density [9, 10]. It was discussed in [9, 10], that when σ_2 has a dominant effect, the system behaves as a Strange metal. For a zero charge density because $\sigma_2 = 0$ we might say that the ALCF behaves similar to $z = 1$ AdS background.

Same as the section 3, we will study the phase transition numerically, in the conducting state, and investigate its' critical exponents.

4.1 Phase transition and critical exponents

Following the previous sections' methodology for our Strange metal, our numerical calculations result in the figure 8. We can see that the same phenomena of phase transition is taking place in here. It was found that the occurance of phase transition phenomena is not governed by the variation of b. So for the ALCF background, the parameter b is showing a quite different characteristics, compared to the previous results in section 3. To study the first order phase transition, again, we should compare the values of energy between three points with a same current density in the low current region, i.e., B, C, D. The energy density would be

$$\mathcal{H} = -\tilde{\mathcal{L}} + \partial_+ a_x \left(\frac{\partial \tilde{\mathcal{L}}}{\partial \, \partial_+ a_x} \right) = \frac{g_{rr}^{1/2}}{r^2} \left(\frac{V}{U} \right)^{1/2} \tag{4.12}$$

Same as the Schrödinger sapcetime from NMT transformation, the point with the higher electric field has a lower energy, hence it is more favorable. This is quite interesting since we'll show that in below, if we turn on the electric field in the light-cone direction, we are getting back the AdS results, which in there, the points with a lower electric field were more favorable.

JHEP01(2019)047

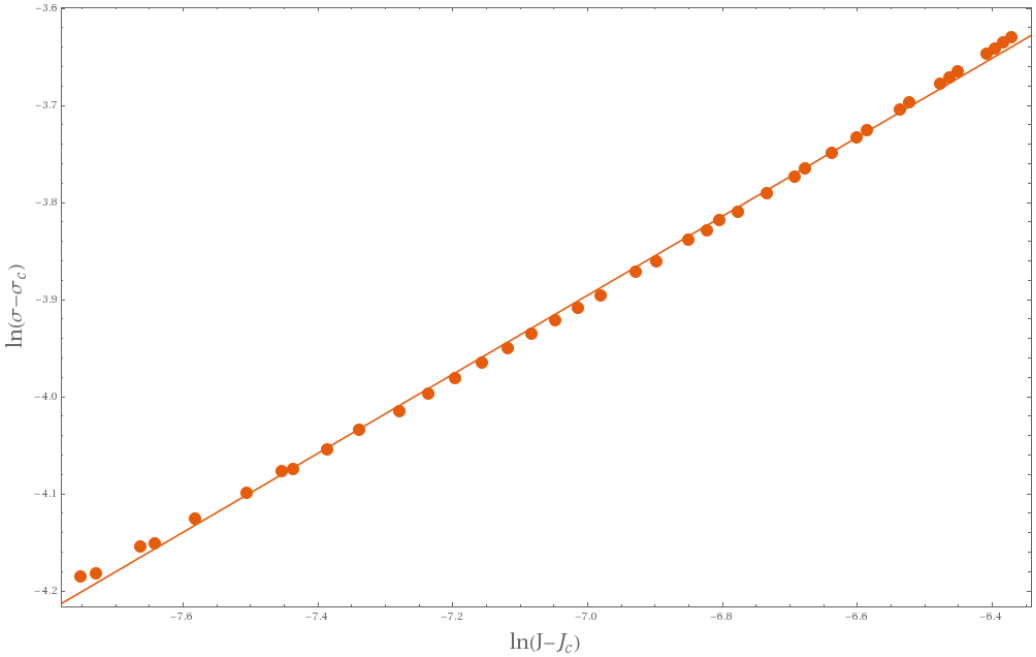

Figure 9. Behaviour of $\ln(\sigma - \sigma_c)$ with the different values of $\ln(J - J_c)$, representing the critical exponent δ for Strange metal. $\delta = 2.25 \pm 0.2$ is computed from the slope of the line presented in the figure.

Following (3.3) and in like manner, critical exponents of β and δ are evaluated for our Strange metal. The numerical results of these exponents can be derived from figure 9 and figure 10. The final result are $\delta = 2.25 \pm 0.2$ and $\beta = 0.47 \pm 0.05$. This was expected due to $z = 1$ behavior of the system at zero charge density.

4.2 Electric field along the light-cone direction

The Legendre transformation of the DBI action of the probe N_f $D7$-branes with the gauge field (2.3) would be

$$S_{D7} = -\int_0^{r_H} dr g_{rr}^{1/2} \sqrt{U(r)\, V(r)}, \tag{4.13}$$

where

$$\begin{aligned} g_{rr} &= \frac{1}{r^2 f(r)} + \theta'^2, \\ U(r) &= \frac{r^4}{f(r)} \left(-4b^4 g_{++}\, E_b^2 + 4b^2 E_b^2 g_{+-} - E_b^2 g_{--} + \frac{f(r)}{r^6} \right) , \\ V(r) &= \frac{\mathcal{N}^2 f(r) \cos^6\theta}{r^6} - \langle J^x \rangle^2 \ . \end{aligned} \tag{4.14}$$

The world-volume horizon is located at r_*, where both U and V are zero,

$$V(r_*) = 0 \to \langle J^x \rangle^2 = \frac{\mathcal{N}^2 f(r_*) \cos^6\theta(r_*)}{r_*^6}, \tag{4.15a}$$

JHEP01(2019)047

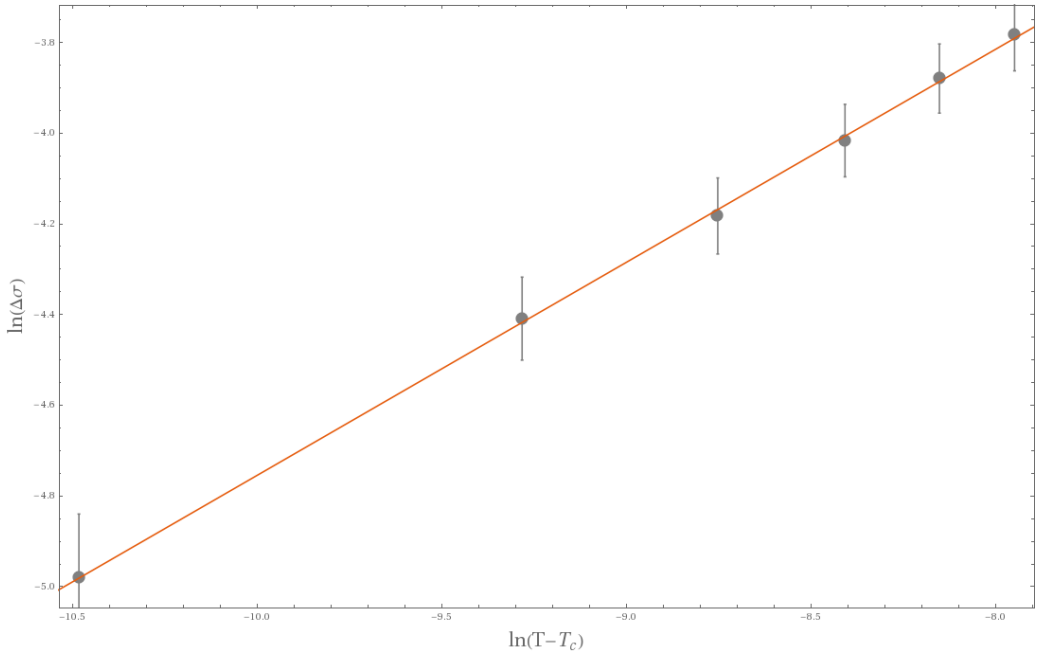

Figure 10. Behaviour of $\ln(\Delta\sigma)$ with the different values of $\ln(T - T_c)$, represnting the critical exponent β for strange metal. $\beta = 0.47 \pm 0.05$ is computed from the slope of the line presented in the figure.

$$U(r_*) = 0 \rightarrow E_b^2 = \frac{f(r_*)}{4\, b^2\, r_*^4}\,. \tag{4.15b}$$

Recalling $E = 2b\, E_b$ (4.15), these equations will give us the world-volume horizon and also the DC conductivity as same as the AdS results [2]. Hence in here, the phase transition from NDC to PDC is the same as AdS background, see [15, 17]. This is quite trivial since we've made a change of coordinate in the metric and gauge field at the same time, therefore the effective action or DBI action remained unchanged.

5 Notes on numerical calculation

As it was mentioned earlier, with the increment of the temperature, before reaching the first-order transition, there exists a second-order transition, which contains a single point called critical point, with a diverging $\frac{\partial E}{\partial J}$. Although the accuracy of J-E curves is important in this work, our numerical analysis points out that for the calculation of critical exponents, the precise indication of the critical point plays the most important factor on the precision of our reported critical exponents.

Authors believe, due to the high sensitivity of critical exponents to the determination of the positions of critical points, current and previous numerical reports of the critical exponents [15, 17], are still doubtful, and a better definition for the critical points is required for a further, more precise investigation. Furthermore, because of the existence of some numerical difficulties, specially in some spacetimes including Schrödinger spacetime, a better numerical technique is also demanded to indicate the critical points.

JHEP01(2019)047

Critical Exponents	NMT	ALCF	AdS [17]
δ	1.54 ± 0.1	2.25 ± 0.2	3.008 ± 0.032
β	0.28 ± 0.1	0.47 ± 0.05	0.505 ± 0.008

Table 2. Summary of the calculated critical exponents.

6 Conclusion

In the QFT with $z = 2$ Schrödinger symmetry, we study the non-equilibrium phase transition by using holographic probe branes. Following [14, 15, 17], using the numerical analysis, we show that the phase transition could occur in the conductor state. For Schrödinger solution from type IIB supergravity, we saw that both background temperature and chemical potential (or rapidity) control the phase structure of the transition.

We have also seen that the same phenomena happens in the probe branes in Schrödinger spacetime from ALCF but interestingly, unlike the solutions from NMT, the phase transition did not take any effect from the variation of chemical potential.

Other than this, it was shown that in all of our spacetimes, for the low current density region of the first order phase transitions, the higher electric fields were energetically more favorable. This was particulary interesting for our Strange metal, because when electric field was in the light-cone direction, we were getting back the AdS results, which in there, the points with a lower electric field were more favorable.

Critical exponents were also calculated for NMT and ALCF. These results, with the addition of the results from [17], are concluded in the following table.

We propose a relation between the dynamical critical exponent z, and δ and β in our Schrödinger spacetime from NMT. As it can be seen from table 2, for our $z = 2$ NMT, the critical exponents are half the values of AdS ones. Therefore, we propose that $\delta_z = \frac{\delta_{\text{AdS}}}{z}$. A further investigation on a more general scale invariant theory with dynamical critical exponent z is carried on [29].

With the study of the critical exponents, we show that ALCF has a phase structure similar to the relativistic theory from AdS background. From table 2, the difference between the value of δ for ALCF and AdS is visible. As it is already discussed in section 5, this difference might be a result of the numerical inaccuracies in the determination of the critical points. A further investigation is needed for a better definition of the critical points, and regarding the numerical techniques used to precisely determine these points in any spacetime.

References

[1] S. Kobayashi et al., *Holographic phase transitions at finite baryon density*, *JHEP* **02** (2007) 016 [hep-th/0611099] [INSPIRE].

JHEP01(2019)047

[2] A. Karch and A. O'Bannon, *Metallic AdS/CFT*, *JHEP* **09** (2007) 024 [arXiv:0705.3870] [INSPIRE].

[3] A. Karch and E. Katz, *Adding flavor to AdS/CFT*, *JHEP* **06** (2002) 043 [hep-th/0205236] [INSPIRE].

[4] M. Ammon, C. Hoyos, A. O'Bannon and J.M.S. Wu, *Holographic flavor transport in Schrödinger spacetime*, *JHEP* **06** (2010) 012 [arXiv:1003.5913] [INSPIRE].

[5] D.T. Son, *Toward an AdS/cold atoms correspondence: a geometric realization of the Schrödinger symmetry*, *Phys. Rev.* **D 78** (2008) 046003 [arXiv:0804.3972] [INSPIRE].

[6] K. Balasubramanian and J. McGreevy, *Gravity duals for non-relativistic CFTs*, *Phys. Rev. Lett.* **101** (2008) 061601 [arXiv:0804.4053] [INSPIRE].

[7] J. Maldacena, D. Martelli and Y. Tachikawa, *Comments on string theory backgrounds with non-relativistic conformal symmetry*, *JHEP* **10** (2008) 072 [arXiv:0807.1100] [INSPIRE].

[8] B.S. Kim and D. Yamada, *Properties of Schroedinger black holes from AdS space*, *JHEP* **07** (2011) 120 [arXiv:1008.3286] [INSPIRE].

[9] B.S. Kim, E. Kiritsis and C. Panagopoulos, *Holographic quantum criticality and strange metal transport*, *New J. Phys.* **14** (2012) 043045 [arXiv:1012.3464] [INSPIRE].

[10] K.B. Fadafan, *Strange metals at finite 't Hooft coupling*, *Eur. Phys. J.* **C 73** (2013) 2281 [arXiv:1208.1855] [INSPIRE].

[11] K.-Y. Kim and D.-W. Pang, *Holographic DC conductivities from the open string metric*, *JHEP* **09** (2011) 051 [arXiv:1108.3791] [INSPIRE].

[12] K. Hashimoto and T. Oka, *Vacuum instability in electric fields via AdS/CFT: Euler-Heisenberg lagrangian and planckian thermalization*, *JHEP* **10** (2013) 116 [arXiv:1307.7423] [INSPIRE].

[13] A. Vahedi, *Ground State Instability in Non-relativistic QFT and Euler-Heisenberg Lagrangian via Holography*, arXiv:1710.05309 [INSPIRE].

[14] S. Nakamura, *Negative differential resistivity from holography*, *Prog. Theor. Phys.* **124** (2010) 1105 [arXiv:1006.4105] [INSPIRE].

[15] S. Nakamura, *Nonequilibrium phase transitions and nonequilibrium critical point from AdS/CFT*, *Phys. Rev. Lett.* **109** (2012) 120602 [arXiv:1204.1971] [INSPIRE].

[16] M. Ali-Akbari and A. Vahedi, *Non-equilibrium phase transition from AdS/CFT*, *Nucl. Phys.* **B 877** (2013) 95 [arXiv:1305.3713] [INSPIRE].

[17] M. Matsumoto and S. Nakamura, *Critical exponents of nonequilibrium phase transitions in AdS/CFT correspondence*, *Phys. Rev.* **D 98** (2018) 106027 [arXiv:1804.10124] [INSPIRE].

[18] H.-B. Zeng and H.-Q. Zhang, *Universal critical exponents of nonequilibrium phase transitions from holography*, *Phys. Rev.* **D 98** (2018) 106024 [arXiv:1807.11881] [INSPIRE].

[19] J. Casalderrey-Solana et al., *Gauge/string duality, hot QCD and heavy ion collisions*, arXiv:1101.0618 [INSPIRE].

[20] T. Albash, V.G. Filev, C.V. Johnson and A. Kundu, *Quarks in an external electric field in finite temperature large N gauge theory*, *JHEP* **08** (2008) 092 [arXiv:0709.1554] [INSPIRE].

[21] A. Kundu and S. Kundu, *Steady-state physics, effective temperature dynamics in holography*, *Phys. Rev.* **D 91** (2015) 046004 [arXiv:1307.6607] [INSPIRE].

JHEP01(2019)047

[22] A. Kundu, *Effective temperature in steady-state dynamics from holography*, *JHEP* **09** (2015) 042 [arXiv:1507.00818] [INSPIRE].

[23] A. Banerjee, A. Kundu and S. Kundu, *Flavour fields in steady state: stress tensor and free energy*, *JHEP* **02** (2016) 102 [arXiv:1512.05472] [INSPIRE].

[24] K. Hashimoto, N. Iizuka and T. Oka, *Rapid thermalization by baryon injection in gauge/gravity duality*, *Phys. Rev.* **D 84** (2011) 066005 [arXiv:1012.4463] [INSPIRE].

[25] C.A. Fuertes and S. Moroz, *Correlation functions in the non-relativistic AdS/CFT correspondence*, *Phys. Rev.* **D 79** (2009) 106004 [arXiv:0903.1844] [INSPIRE].

[26] A. Volovich and C. Wen, *Correlation functions in non-relativistic holography*, *JHEP* **05** (2009) 087 [arXiv:0903.2455] [INSPIRE].

[27] M. Taylor, *Non-relativistic holography*, arXiv:0812.0530 [INSPIRE].

[28] M. Guica, K. Skenderis, M. Taylor and B.C. van Rees, *Holography for Schrödinger backgrounds*, *JHEP* **02** (2011) 056 [arXiv:1008.1991] [INSPIRE].

[29] A. Vahedi , M. Shakeri and D. Zolfaghari, *Effect of dynamical critical exponents on non-equilibrium critical exponent*, work in progress.

JHEP01(2019)047